Rapid Communications

Dualism of the 4f electrons and its relation to high-temperature antiferromagnetism in the heavy-fermion compound $YbCoC_2$

D. A. Salamatin,[1,2] N. Martin,[3] V. A. Sidorov,[1] N. M. Chtchelkatchev,[1,4] M. V. Magnitskaya,[1,5] A. E. Petrova,[1,5] I. P. Zibrov,[1] L. N. Fomicheva,[1] Jing Guo,[6] Cheng Huang,[6] Liling Sun,[6] and A. V. Tsvyashchenko[1,*]

[1]*Institute for High Pressure Physics, Russian Academy of Sciences, 14 Kaluzhskoe shosse, 108840 Troitsk, Russia*

[2]*Joint Institute for Nuclear Research, 141980 Dubna, Moscow Region, Russia*

[3]*Université Paris-Saclay, CNRS, CEA, Laboratoire Léon Brillouin, 91191 Gif-sur-Yvette, France*

[4]*Ural Federal University, 19 Mira str., 620002 Ekaterinburg, Russia*

[5]*P.N. Lebedev Physical Institute of the Russian Academy of Sciences, 53 Leninskiy prospekt, 119991 Moscow, Russia*

[6]*Institute of Physics, Chinese Academy of Sciences, 100190 Beijing, People's Republic of China*

(Received 25 December 2019; revised manuscript received 2 March 2020; accepted 3 March 2020; published 18 March 2020)

We report on the study of the noncentrosymmetric ternary carbide $YbCoC_2$. Our magnetization, specific heat, resistivity, and neutron diffraction measurements consistently show that the system behaves as a heavy-fermion compound, displaying an amplitude-modulated magnetic structure below the Néel temperature reaching $T_N =$ 33 K under pressure. Such a large value, being the highest among the Yb-based systems, is explained in the light of our *ab initio* calculations, which show that the 4f electronic states of Yb have a dual nature, i.e., due to their strong hybridization with the 3d states of Co, 4f states expose both localized and itinerant properties.

DOI: 10.1103/PhysRevB.101.100406

The dual nature of the 5f and 4f electrons, i.e., the coexistence of localized and itinerant states in a variety of actinide and rare-earth (RE) heavy-fermion systems (e.g., UPt_3, UPd_2Al_3 [1], UGe_2 [2–4], $PuCoGa_5$ [5], $YbRh_2Si_2$ [6], $YbAl_3$ [7]) is the subject of an intense discussion. A theory for the electronic excitations in uranium compounds, based on the localization of two 5f electrons, was developed by Zwicknagl and Fulde [8]. The standard model for 4f electrons in RE metals and their compounds is that an integral number of 4f electrons are assumed being localized at each RE ion site. This applies to both "normal" REs, where a single 4f configuration of given occupation is stable, and to mixed-valent cases, where fluctuations between states with different integral 4f occupations take place. The nature of magnetism (itinerant or localized) and the competition between ordered and disordered ground states in these mixed-valent ("abnormal") RE elements (Ce, Eu, and Yb), remain a major challenge in condensed matter physics. In this context, the Kondo effect and the Ruderman-Kittel-Kasuya-Yosida (RKKY) interaction arising between itinerant and localized 4f electrons play essential roles, as originally pointed out by Doniach [9].

The noncentrosymmetric carbide $YbCoC_2$, first synthesized more than 30 years ago [10], represents an interesting platform for studying such physics. Here, we report on the study of its bulk magnetic and transport properties at ambient and elevated pressure, complemented by neutron diffraction measurements and *ab initio* calculations. We show that $YbCoC_2$ is a heavy-fermion compound with an amplitude modulated incommensurate magnetic order. Its Néel temperature is the highest among Yb^{3+}-based systems, exceeding the previous record value belonging to β-$YbAlB_4$ [11]. Taken together, our experimental and numerical results indicate that the dual nature of the 4f electrons is essential for understanding the magnetic and transport properties of $YbCoC_2$.

The transition from localized to itinerant electron states signaling the onset of long-range electronic correlations, is also of great interest. In lanthanides this effect is related to Ce, the first element with a single 4f-electron level. The Yb intermetallic compounds are usually considered as being dominated by two valence states, where Yb^{3+} ions can be seen as f-hole analogs of Ce. Owing to such an electronic configuration, one can anticipate a dual character of 4f states in $YbCoC_2$, with transitions from localized states to itinerant ones. Heavy-fermion magnetism in Yb-based systems with localized 4f electrons mainly occurs in compounds where the ordering temperature is low (typically, $T_N < 10$ K), for instance in $YbNi_2$ [12], YbNiSn [13], YbPtGe [14,15], YbPdGe [15,16], or $YbRh_2Si_2$ [17], YbPtBi [18,19]. In fact, in many such compounds displaying antiferromagnetic (AFM) order, T_N is even below 1 K (e.g., $YbIr_2$ [20], YbPd [21], YbX (X = N, P, As) [22], and YbXCu$_2$ (X = Au, Pd) [23]). [A few exceptions are $YbBe_{13}$ ($T_N = 1.3$ K) [24], Yb_3Pd_4 ($T_N = 3$ K) [25], and YbB_2 ($T_N = 5.7$ K) [26].] At atmospheric pressure, the highest magnetic transition temperature is $T_N = 20$ K observed recently in α-$YbAl_{1-x}Mn_xB_4$ for $x = 0.27$ [27]. The pressure-induced magnetic ordering was found in the heavy-fermion superconductor β-$YbAlB_4$ [28], where the magnetic transition temperature increases up to 32 K, obtained under the external pressure P of 8 GPa [11].

*tsvyash@hppi.troitsk.ru

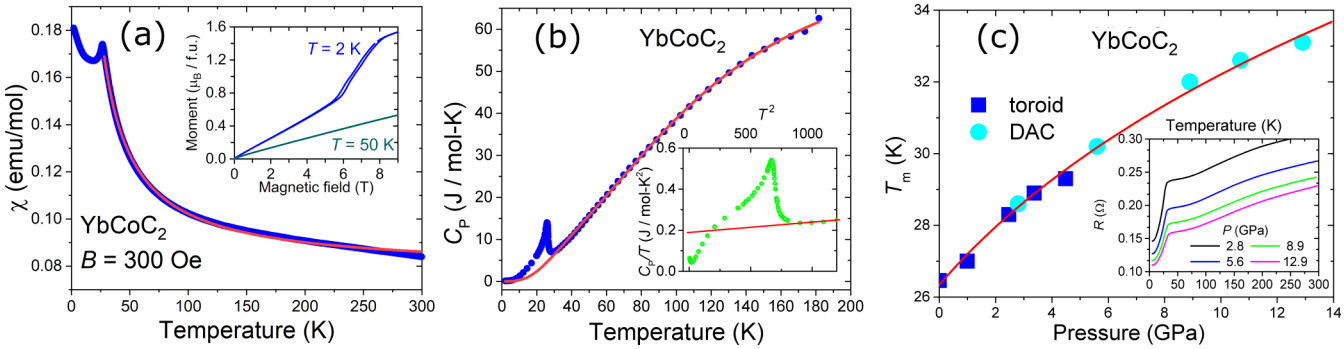

FIG. 1. (a) Temperature dependence of the magnetic susceptibility χ of $YbCoC_2$, measured in the external magnetic field $B = 300$ Oe (blue points). The red line is the fit of a modified Curie-Weiss law to the $T = 28$–300 K data (see the text for details). Inset: isothermal magnetization of $YbCoC_2$ measured in the $B = 0$–9 T field range at $T = 2$ and 50 K. (b) Temperature dependence of the heat capacity C_P of $YbCoC_2$ (blue points). The red line is the fit of two Debye laws to the high-temperature data, extrapolated down to $T \to 0$ (see the text). Inset: the low-temperature part of C_P/T vs T^2. The red line is the linear approximation of C_P/T vs T^2 extended down to 0 K. (c) Pressure dependence of the magnetic transition temperature T_m measured in the toroid and diamond-anvil (DAC) high-pressure cells (blue squares and light-blue circles, respectively). The red line is the approximation with the function $f(P - P_{c0})^{\alpha}$, where $f = 18.6$ K/GPa$^{1/5}$, $P_{c0} = -5.7$ GPa, and $\alpha = 1/5$. Inset: temperature dependence of the isobaric electrical resistance, measured at $P = 2.8$–12.9 GPa.

Previously it has been established that the magnetic structure of the $RCoC_2$ compounds (where R is a heavy RE element), isostructural to $YbCoC_2$, is ferromagnetic (FM). The magnetic moments usually point along the a axis [29], except in $DyCoC_2$ where they lie in the ac plane [30]. The magnetic susceptibility measurements in $YCoC_2$ and the refinements of neutron powder diffraction patterns of other $RCoC_2$ compounds indicate that the Co and C ions are nonmagnetic [30,31]. Notably, the Curie temperature for $RCoC_2$ compounds deviates from the de Gennes law [29,32], indicating the importance of the interactions beyond RKKY in the stabilization of the magnetic order in this series and calls for further studies of the nature of magnetism in these systems.

Polycrystalline samples of $YbCoC_2$ were synthesized by melting Yb, Co, and C (see Ref. [33]) at 8 GPa and 1500–1700 K using a Toroid high-pressure cell. The Rietveld analysis of x-ray and neutron diffraction data at $T = 300$ K shows that the compound crystallizes in an orthorhombic structure of the $CeNiC_2$-type (space group $Amm2$, No. 38), similar to other RE carbides $RCoC_2$. High-pressure x-ray diffraction measurements performed at the 15U beamline of the Shanghai Synchrotron Radiation Facility (China) show that the orthorhombic crystal structure is preserved up to 37 GPa [34]. A fit of a Murnaghan equation of state volume vs pressure data yields a bulk modulus $B_0 = 176(23)$ GPa, with its first pressure derivative $B_0' = 9(1)$. The bulk magnetic properties of $YbCoC_2$ were studied by vibrating sample magnetometry using a physical property measurement system. The electrical resistivity measurements were performed on bulk polycrystalline samples using a lock-in detection technique [35]. The high-pressure resistance measurements below 5 GPa were performed in a miniature clamped Toroid-type device with glycerine-water (3:2) liquid as the pressure transmitting medium. For higher pressures a diamond-anvil cell (DAC) with NaCl as the pressure transmitting medium was used.

The magnetic susceptibility $\chi(T)$ measured in the magnetic field $B = 300$ Oe exhibits a sharp peak, indicative of an AFM-like transition at $T_N = 25.6(2)$ K [Fig. 1(a)]. In the $T = 28$–300 K range, $\chi(T)$ can be well described by a modified Curie-Weiss law $\chi = \chi_0^* + C^*/(T - \theta)$, where χ_0^* is a temperature-independent term, C^* is the Curie constant, and θ is the Weiss constant. The effective magnetic moment deduced from this approximation is $\mu_{eff} = 4.31(1)\mu_B$ per formula unit (f.u.), a value close to that of the free Yb^{3+} ion ($4.54\mu_B$). The small positive Weiss constant $\theta = 2.4(1)$ K reveals the presence of weak ferromagnetic correlations and a small value of the ratio $f_s = \theta/T_N \approx 0.09 \ll 1$ indicates a weak level of spin frustration in the system.

The inset of Fig. 1(a) shows field dependences of the bulk magnetization M measured in the $B = 0$–9 T range at $T = 2$ and 50 K. At $T = 50$ K, $M(H)$ has a smooth linear character, typical of a paramagnet. In contrast, the curve measured at $T = 2$ K $< T_N$ first increases linearly up to $\approx$6 T, until a "spin-flop"-like transition with a hysteresis of about 0.2 T takes place in the $\approx$6–8 T range. M does not fully saturate at the highest field of 9 T and reaches a value of $\approx 1.6\mu_B$/f.u., which stands well below the theoretical saturation moment for the full Yb^{3+} multiplet ($\mu_s = 4.0\mu_B$).

Figure 1(b) displays the temperature dependence of the heat capacity C_P, obtained in the 2–180 K range. Around T_N, the $C_P(T)$ curve exhibits a lambda anomaly, with a maximum at $\approx$26 K, which is consistent with the bulk AFM-like transition deduced from the $\chi(T)$ data. The heat capacity jump at T_N is equal to $\Delta C_P(T_N) = 14.64$ J/mol K. This value is close to the one calculated for an amplitude modulated magnetic structure for Yb^{3+}, namely, 13.43 J/mol K [36]. The heat capacity at $T > 30$ K was approximated by $C_{fit}(T) = m_1 D(T, \Theta_1) + m_2 D(T, \Theta_2)$, where D is the Debye function, with the characteristic temperatures $\Theta_1 = 516(11)$ K and $\Theta_2 = 176(7)$ K. The best fit was obtained with the coefficients $m_1 = 2.49(4)$ and $m_2 = 0.79(5)$. The magnetic entropy of the transition computed according to $S_m(T) = \int_{1.9\,K}^{T} C_m(T)/T\,dT$, where $C_m(T) = C_P(T) - C_{fit}(T)$ is the magnetic part of heat capacity, amounts to 3.91 J/mol K at $T = 30$ K. This value is about 70% of that expected for a magnetic doublet ground

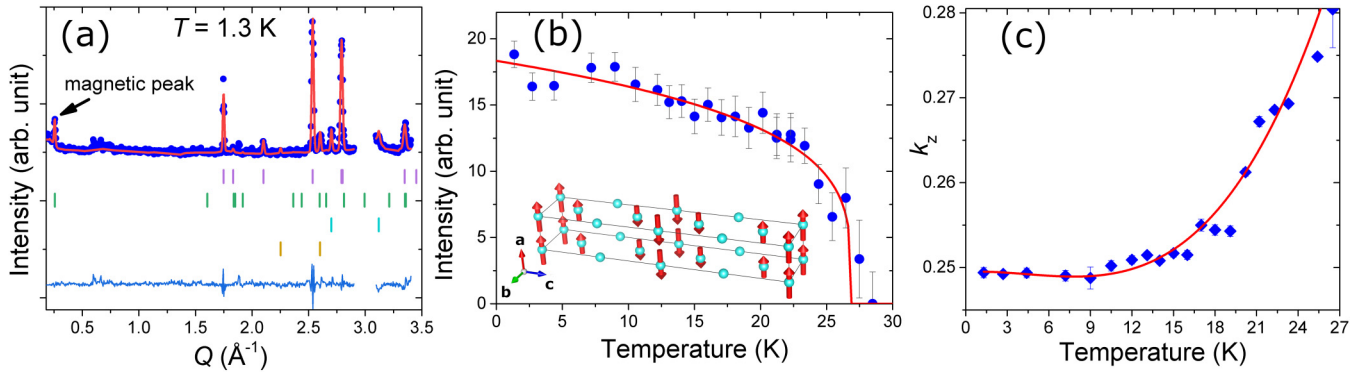

FIG. 2. (a) Refined neutron powder-diffraction pattern of $YbCoC_2$ measured at $T = 1.3$ K and ambient pressure: the experimental points (blue dots), the calculated profiles (red line), and their difference (light-blue line). The bars in the lower part of the graph represent the calculated Bragg reflections that correspond to the nuclear *Amm*2 structure (first row, purple), the magnetic phase (second row, green), the aluminum container (third row, cyan), and the nonmagnetic impurity phase YbO (fourth row, brown). (b) Temperature dependence of the square root of the integrated intensity of the magnetic peak (blue circles). The red line is the power-law fit (see the text). Inset: schematic representation of the magnetic unit cell of $YbCoC_2$ in the commensurate phase (only Yb magnetic atoms are shown). (c) Temperature dependence of the k_z component of the magnetic wave vector (blue diamonds). The red line is drawn to guide the eye.

state and is most likely due to Kondo screening [37]. The Sommerfeld coefficient obtained from the C_P data just above T_N is $\gamma = 190(1)$ mJ/mol K^2 [see inset of Fig. 1(b)]. This value suggests a considerable enhancement of the effective electron mass in $YbCoC_2$ comparable with other heavy-fermion compounds [38,39]. The low-temperature upturn in C_P/T [see the inset of Fig 1(b)] indicates that there is a possibility of the second magnetic transition in $YbCoC_2$ similar to the incommensurate-commensurate magnetic transition in $CeNiC_2$ [39].

As shown in Fig. 1(c), the electrical resistance increases monotonically with temperature revealing the metallic character of $YbCoC_2$. Because of the coherent scattering of charge carriers in the magnetically ordered state, the resistance drops down below the AFM-like transition temperature [see inset of Fig. 1(c)]. Interestingly, the transition temperature T_m, determined from the onset of the resistance, increases with external pressure up to 33.2(3) K at $P = 13$ GPa.

In order to elucidate the magnetic structure of $YbCoC_2$, we have used neutron powder diffraction on the thermal instrument G4-1 (Laboratoire Léon Brillouin). The low-temperature patterns display an additional peak at low angles [see Fig. 2(a)]. The square- root of the integrated intensity of this peak depends on temperature [see Fig. 2(b)] and may be approximated with the function $\sigma_0(1 - T/T_C)^\beta$, with the critical exponent $\beta = 0.24(4)$ and the critical temperature $T_C = 26.9(7)$ K. This peak can be indexed with the wave vector $(0, 0, k_z)$, where k_z is temperature dependent [see Fig. 2(c)]. The best refinement of the magnetic part of the neutron powder diffraction pattern is achieved by assuming an amplitude modulated (sine-wave) structure of Yb^{3+} magnetic moments, pointing along the a axis with the amplitude $1.32(7)\mu_B$ at $T = 1.3$ K. Such a value of magnetic moment is typical for Yb in magnetic compounds [15,19,40,41] and may be attributed to the crystal electric field effects and a partial screening due to the Kondo mechanism. The structure locks into a commensurate state with $k_z = 1/4$ at $T_{\text{lock-in}} \approx 8$ K.

The *ab initio* simulations of $YbCoC_2$ were performed using the WIEN2K package [42] within the density functional theory (DFT) and the local-density approximation (LDA), with the spin-orbit coupling taken into account. The 4f electrons of the Yb ion were explicitly treated as valent and not completely localized, and as such were allowed to hybridize with all other states. The calculations started from the experimental lattice parameters measured in this work, with subsequent relaxation of internal atomic coordinates. In these initial DFT-LDA calculations ($T = 0$ K), a nonmagnetic (paramagnetic) ground state of $YbCoC_2$ was determined, whereas no magnetic solution turned out to be stable.

From the band structure and density of states (DOS) of paramagnetic $YbCoC_2$ it follows [34] that 4f states of Yb are present at the Fermi energy (E_F), and the main contribution to the total DOS at E_F stems from the strongly hybridized ytterbium f and cobalt d states. The energy bands in the vicinity of E_F are flat, which indicates a strong enhancement of the electron mass to a value typical for heavy-fermion systems.

To treat strong electron correlations in the Yb 4f shell adequately, we further employed the combination of DFT-LDA [42] and dynamical mean-field theory (DMFT) [43] as implemented in the EDMFT package [44]. Since the DMFT method is not applicable to the low-temperature region, for simulations of the magnetic state of $YbCoC_2$ observed experimentally below 30 K we have used the LDA+U approach [45,46] in the WIEN2K implementation, which can perform zero-temperature calculations with accounting for correlation effects of 4f electrons.

The band structure and DOS computed at $T = 250$ K using DMFT are shown in Figs. 3(a) and 3(b). The evaluated number of 4f electrons is about 13.05, i.e., the valence of Yb is actually equal to three. There is a certain similarity between the DFT and DMFT results in the number of 4f electrons and in the position of the bands and corresponding DOS peaks [34]. Within both approaches, the Fermi energy falls into a steep slope of the 4f DOS whose maximum is very close to E_F. Apparently, the proximity of the 4f peak to E_F and the resulting relatively high $N(E_F)$, as well as a significant f-d hybridization favor the high magnetic transition temperature for $YbCoC_2$.

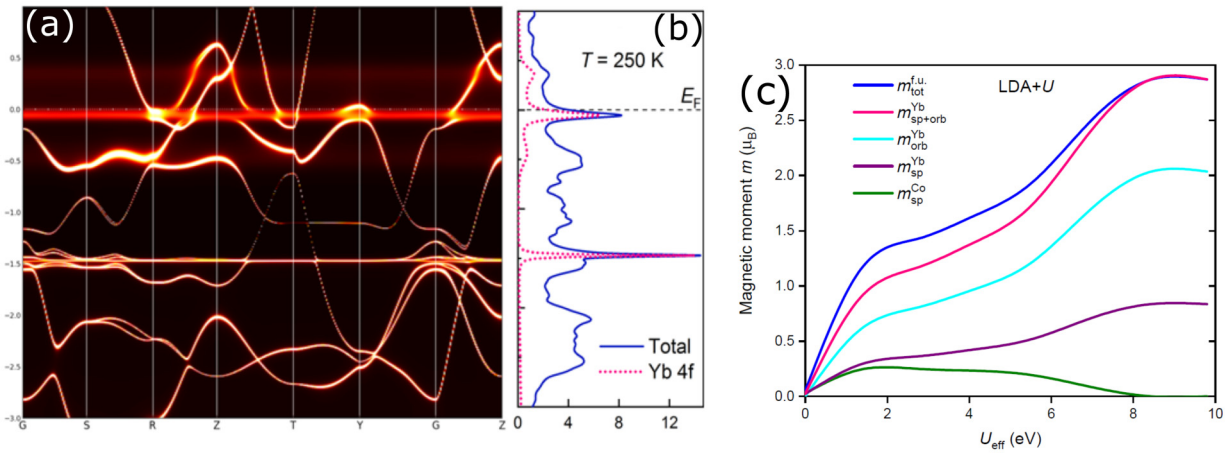

FIG. 3. The DMFT band structure (a) and DOS (b) at $T = 250$ K. The DOS is in arb. units and the Fermi energy is set to zero. (c) The LDA+U calculations: the magnetic moment per formula unit and its partial contributions as functions of U_{eff}. The green line is the spin moment of Co, the violet line is the spin moment of Yb, the cyan line is the orbital moment of Yb, the red line is the total moment of Yb, and the blue line is the total magnetic moment.

In our LDA+U simulations of the magnetic state only the $4f$-electron correlations were taken into account. The positions of the bands are found to shift downwards with increasing $U_{\text{eff}} = U - J$ (where U and J are the standard on-site Coulomb interaction constants). We obtained a stable FM ordering with the periodicity of the crystal lattice. The total magnetic moment and its main partial atomic contributions as functions of U_{eff} are depicted in Fig. 3(c). The largest partial contribution (including both the spin and orbital terms) is μ_{Yb} directed along the a axis in accordance with the experimental data and drawn in Fig. 3(c) as the red line. This is the magnetic moment of the Yb site which increases with U_{eff}. The magnetic moment of Co is smaller tending to zero with increasing U_{eff}, whereas the magnetic moments at carbon sites and in the interstitial region are negligible at any U_{eff}.

The interval of U_{eff} between 1.3 and 3.5 eV has been considered as optimal, corresponding to the experimental situation. The change in U_{eff} in this interval does not lead to a strong variation of the magnetic moments and band positions. The Yb moment varies from 0.9 to 1.3μ_{B}, which correlates well with the experimental observations. The model of ferromagnetic alignment used in the calculations turned out to be quite reasonable, because the period of experimental modulated magnetic structure is about four times that of the crystal lattice. Moreover the Yb magnetic moments are codirected to each other within the crystallographic unit cell [see the inset in Fig. 2(b)]. Thus, our LDA+U calculations demonstrate that $YbCoC_2$ possesses a stable magnetic ordering with the magnetization predominantly located at the Yb sites.

A wealth of experimental and numerical results presented in this study unambiguously establishes that the noncentrosymmetric $YbCoC_2$ is an unusual heavy-fermion system, displaying incommensurate antiferromagnetic ordering with the transition temperature reaching 33 K under pressure. The nature of its magnetic structure is surprising in itself, since the isostructural compounds $RCoC_2$ (where $R =$ Gd-Tm) display FM ordering. This fact is well captured by our *ab initio* calculations, which also reproduce the direction of the Yb magnetic moments and, quantitatively, their amplitude. As a key result, we reveal a strong hybridization between the $4f$ states of Yb and the $3d$ orbitals of Co. We believe that this feature is instrumental in explaining the robustness of the magnetic order and its enhancement under applied external pressure. Another appealing finding concerns the evolution of the magnetic structure with pressure. Indeed, a fine-tuning of the tight competition between RKKY and Kondo interactions is a well-proven route towards the observation of quantum criticality, exotic forms of superconductivity, and novel strange metallic states.

This work was supported by Russian Science Foundation: D.A.S., V.A.S., A.E.P., and A.V.T. acknowledge the support of their experimental work (RSF Grant No. 17-12-01050); N.M.C. and M.V.M. are grateful for support of their theoretical calculations (RSF Grant No. 18-12-00438). The results of calculations were obtained using the computational resources of MCC NRC "Kurchatov Institute" [53] and supercomputers at Joint Supercomputer Center of RAS (JSCC RAS). We also thank the Uran supercomputer of IMM UB RAS for access.

[1] T. Takahashi, N. Sato, T. Yokoya, A. Chainani, T. Morimoto, and T. Komatsubara, J. Phys. Soc. Jpn. **65**, 156 (1996).

[2] R. Troć, Z. Gajek, and A. Pikul, Phys. Rev. B **86**, 224403 (2012).

[3] A. Yaouanc, P. Dalmas de Réotier, P. C. M. Gubbens, C. T. Kaiser, A. A. Menovsky, M. Mihalik, and S. P. Cottrell, Phys. Rev. Lett. **89**, 147001 (2002).

[4] F. Haslbeck, S. Säubert, M. Seifert, C. Franz, M. Schulz, A. Heinemann, T. Keller, P. Das, J. D. Thompson, E. D. Bauer, C. Pfleiderer, and M. Janoschek, Phys. Rev. B **99**, 014429 (2019).

[5] C. Booth, Y. Jiang, D. Wang, J. Mitchell, P. Tobash, E. Bauer, M. Wall, P. Allen, D. Sokaras, D. Nordlund, T.-C. Weng, M. Torrez, and J. Sarrao, Proc. Natl. Acad. Sci. USA **109**, 10205 (2012).

[6] S. Danzenbächer, D. V. Vyalikh, K. Kummer, C. Krellner, M. Holder, M. Höppner, Y. Kucherenko, C. Geibel, M. Shi, L. Patthey, S. L. Molodtsov, and C. Laubschat, Phys. Rev. Lett. **107**, 267601 (2011).

[7] T. Ebihara, Y. Inada, M. Murakawa, S. Uji, C. Terakura, T. Terashima, E. Yamamoto, Y. Haga, Y. Ōnuki, and H. Harima, J. Phys. Soc. Jpn. **69**, 895 (2000).

[8] G. Zwicknagl and P. Fulde, J. Phys.: Condens. Matter **15**, S1911 (2003).

[9] S. Doniach, Physica B+C **91**, 231 (1977).

[10] W. Jeitschko and M. Gerss, J. Less-Common Met. **116**, 147 (1986).

[11] T. Tomita, K. Kuga, Y. Uwatoko, and S. Nakatsuji, Phys. Rev. B **94**, 245130 (2016).

[12] D. P. Rojas, L. Fernández Barquín, C. Echevarria-Bonet, and J. Rodríguez Fernández, Solid State Commun. **152**, 1834 (2012).

[13] M. Kasaya, H. Suzuki, T. Yamaguchi, and K. Katoh, J. Phys. Soc. Jpn. **61**, 4187 (1992).

[14] K. Katoh, S. Nakagawa, G. Terui, and A. Ochiai, J. Phys. Soc. Jpn. **78**, 104721 (2009).

[15] N. Tsujii, K. Katoh, L. Keller, A. Dönni, N. Terada, and H. Kitazawa, J. Phys.: Condens. Matter **27**, 325601 (2015).

[16] K. Enoki, Y. Hirose, S. Yoshiuchi, K. Sugiyama, F. Honda, T. Takeuchi, E. Yamamoto, Y. Haga, M. Hagiwara, K. Kindo, R. Settai, and Y. Ōnuki, J. Phys. Soc. Jpn. **81**, SB056 (2012).

[17] P. Gegenwart, J. Custers, C. Geibel, K. Neumaier, T. Tayama, K. Tenya, O. Trovarelli, and F. Steglich, Phys. Rev. Lett. **89**, 056402 (2002).

[18] Z. Fisk, P. C. Canfield, W. P. Beyermann, J. D. Thompson, M. F. Hundley, H. R. Ott, E. Felder, M. B. Maple, M. A. Lopez de la Torre, P. Visani, and C. L. Seaman, Phys. Rev. Lett. **67**, 3310 (1991).

[19] B. G. Ueland, A. Kreyssig, K. Prokeš, J. W. Lynn, L. W. Harriger, D. K. Pratt, D. K. Singh, T. W. Heitmann, S. Sauerbrei, S. M. Saunders, E. D. Mun, S. L. Bud'ko, R. J. McQueeney, P. C. Canfield, and A. I. Goldman, Phys. Rev. B **89**, 180403(R) (2014).

[20] J. Willis, J. Smith, and Z. Fisk, J. Magn. Magn. Mater. **47-48**, 581 (1985).

[21] R. Pott, W. Boksch, G. Leson, B. Politt, H. Schmidt, A. Freimuth, K. Keulerz, J. Langen, G. Neumann, F. Oster, J. Röhler, U. Walter, P. Weidner, and D. Wohlleben, Phys. Rev. Lett. **54**, 481 (1985).

[22] H. Ott, H. Rudigier, and F. Hulliger, Solid State Commun. **55**, 113 (1985).

[23] C. Rossel, K. N. Yang, M. B. Maple, Z. Fisk, E. Zirngiebl, and J. D. Thompson, Phys. Rev. B **35**, 1914 (1987).

[24] U. Walter, Z. Fisk, and E. Holland-Moritz, J. Magn. Magn. Mater. **47-48**, 159 (1985).

[25] B. Pollit, D. Dürkop, and P. Weidner, J. Magn. Magn. Mater. **47-48**, 583 (1985).

[26] M. Avila, S. Budko, C. Petrovic, R. Ribeiro, P. Canfield, A. Tsvyashchenko, and L. Fomicheva, J. Alloys Compd. **358**, 56 (2003).

[27] S. Suzuki, K. Takubo, K. Kuga, W. Higemoto, T. U. Ito, T. Tomita, Y. Shimura, Y. Matsumoto, C. Bareille, H. Wadati, S. Shin, and S. Nakatsuji, arXiv:1803.09366 .

[28] T. Tomita, K. Kuga, Y. Uwatoko, P. Coleman, and S. Nakatsuji, Science **349**, 506 (2015).

[29] W. Schäfer, W. Kockelmann, G. Will, J. Yakinthos, and P. Kotsanidis, J. Alloys Compd. **250**, 565 (1997).

[30] H. Amanai, H. Onodera, M. Ohashi, S. Matsuo, H. Yamauchi, Y. Yamaguchi, and N. Sato, J. Magn. Magn. Mater. **148**, 413 (1995).

[31] W. Schäfer, G. Will, P. Kotsanidis, and J. Yakinthos, J. Magn. Magn. Mater. **88**, 13 (1990).

[32] P. G. De Gennes, J. Phys. Radium **23**, 630 (1962).

[33] A. Tsvyashchenko, J. Less-Common Met. **99**, L9 (1984).

[34] See Supplemental Material at http://link.aps.org/supplemental/10.1103/PhysRevB.101.100406 which includes Refs. [47–52], for the additional details on the experimental and computational methods.

[35] A. E. Petrova, V. A. Sidorov, and S. M. Stishov, Phys. B (Amsterdam, Neth.) **359-361**, 1463 (2005).

[36] J. A. Blanco, D. Gignoux, and D. Schmitt, Phys. Rev. B **43**, 13145 (1991).

[37] J. A. Blanco, M. de Podesta, J. I. Espeso, J. C. Gómez Sal, C. Lester, K. A. McEwen, N. Patrikios, and J. Rodríguez Fernández, Phys. Rev. B **49**, 15126 (1994).

[38] S. Katano, K. Shibata, K. Nakashima, H. Yoshimura, and Y. Matsubara, J. Phys. Soc. Jpn. **86**, 104704 (2017).

[39] K. Motoya, K. Nakaguchi, N. Kayama, K. Inari, J. Akimitsu, K. Izawa, and T. Fujita, J. Phys. Soc. Jpn. **66**, 1124 (1997).

[40] S. Chattopadhyay, V. Simonet, V. Skumryev, A. A. Mukhin, V. Y. Ivanov, M. I. Aroyo, D. Z. Dimitrov, M. Gospodinov, and E. Ressouche, Phys. Rev. B **98**, 134413 (2018).

[41] A. Yaouanc, P. D. de Réotier, L. Keller, B. Roessli, and A. Forget, J. Phys.: Condens. Matter **28**, 426002 (2016).

[42] P. Blaha, K. Schwarz, G. Madsen, D. Kvasnicka, J. Luitz, R. Laskowski, F. Tran, and L. Marks, *WIEN2k, An Augmented Plane Wave + Local Orbitals Program for Calculating Crystal Properties* (Karlheinz Schwarz, Techn. Universitat Wien, Austria, 2018).

[43] G. Kotliar, S. Y. Savrasov, K. Haule, V. S. Oudovenko, O. Parcollet, and C. A. Marianetti, Rev. Mod. Phys. **78**, 865 (2006).

[44] K. Haule, C.-H. Yee, and K. Kim, Phys. Rev. B **81**, 195107 (2010).

[45] V. I. Anisimov, I. V. Solovyev, M. A. Korotin, M. T. Czyżyk, and G. A. Sawatzky, Phys. Rev. B **48**, 16929 (1993).

[46] A. I. Liechtenstein, V. I. Anisimov, and J. Zaanen, Phys. Rev. B **52**, R5467 (1995).

[47] H. K. Mao, J. Xu, and P. M. Bell, J. Geophys. Res.: Solid Earth **91**, 4673 (1986).

[48] J. Rodríguez-Carvajal, Phys. B (Amsterdam, Neth.) **192**, 55 (1993).

[49] A. C. Larson and R. B. V. Dreele, Los Alamos National Laboratory Report LAUR 86-748 (2000), https://www.ncnr.nist.gov/xtal/software/gsas.html.

[50] A. H. MacDonald, W. E. Picket, and D. D. Koelling, J. Phys. C: Solid State Phys. **13**, 2675 (1980).

[51] K. Momma and F. Izumi, J. Appl. Crystallogr. **44**, 1272 (2011).

[52] A. Georges, G. Kotliar, W. Krauth, and M. J. Rozenberg, Rev. Mod. Phys. **68**, 13 (1996).

[53] http://computing.nrcki.ru/.